

## Effect of Ni content, temperature on the electrical and colorimetric properties of nano $\text{Ni}_x\text{Zn}_{(1-x)}\text{O}$ blue pigments

M. Khairy<sup>a,b,\*</sup>, N. Magdy<sup>a</sup>, Z. A. Omran<sup>a</sup>

<sup>a</sup>Chemistry Department, Faculty of Science, Benha University, Benha, Egypt

<sup>b</sup>Chemistry Department, College of Science, Imam Mohammad Ibn Saud Islamic University (IMSIU), Riyadh 11623, Saudi Arabia

Nanosized Ni doped ZnO ( $\text{Ni}_x\text{Zn}_{1-x}\text{O}$ , with  $20 \leq x \leq 70$ ) were synthesized by simple co-precipitation method at different calcinations temperature (400, 600, 800 and 1000 °C). All synthesized oxides well characterized by XRD, scanning electron microscopy (SEM). The electrical properties and the colorimetric parameters (CIEL L\* a\* b\*) were measured. The results obviously show that  $\text{Ni}^{2+}$  ions incorporated into the ZnO structure without difficulty. For the highest concentration of  $\text{Ni}^{2+}$  for  $x = 0.40$  and  $0.70$  of  $\text{Ni}^{2+}$  doping, the XRD revealed an extra diffraction peak characteristic to NiO, indicating an upper limit of Ni concentration. The crystallite size was discovered to be between 13 and 109 nm. With the addition of Ni to the ZnO, the temperature dependency of electrical conductivity of samples increases. The temperature dependence of dielectric constant of samples is found to decrease with incorporation of Ni in the solution. The samples show very good blue color with load 20% of Ni.

(Received June 9, 2022; Accepted October 5, 2022)

*Keywords:*  $\text{Ni}_x\text{Zn}_{(1-x)}\text{O}$ , Nanosized, Electrical properties, Colorimetric properties

### 1. Introduction

Nanoparticle of ZnO has versatile properties that are important for application in electronic, photovoltaic, pigment and sensor [1-3]. Zinc oxide has a semiconductor property that allows it to function as a dielectric at low temperatures and as a conductor at high temperatures. The factor that controls the behavior of ZnO is related to atom diffusion during the sintering process, as the energy of the band gap decreases as the temperature of the material increases. Because of the improper packing of the atoms, zinc oxide comprises a large number of grain boundaries, which present a high-energy area. When the amount of grain area in the material is lowered by grain expansion, the overall energy in the material is reduced. The migration of grain boundaries during grain growth allows larger grains to grow at the expense of smaller grains. Diffusion of atoms across grain boundaries is essential for material grain development. To migrate to a new position, the atom must first overcome an energy barrier known as the activation energy ( $E_a$ ), which must be overcome using thermal energy. The kinetics of diffusion are substantially influenced by temperature [4]. The diffusion coefficient increases as the temperature of the substance rises. Doping improves electrical conductivity by allowing current to disperse and transport it. As a result, diffusion is slow at low temperatures, reducing the material's mobility and conductivity [4]. When the diffusion coefficient of a ZnO crystal is low, dielectric polarization occurs due to the presence of atomic and molecular forces, and occurs anytime charges in a material are shifted with respect to one another under the influence of an electric field.

The dielectric constant ( $\epsilon$ ) is computed from the capacitance value, which may be calculated using the equation below.

$$\epsilon = (c / \epsilon_0) (t/A) = (t \times c) / \pi (d/2)^2 \times \epsilon_0 \quad (1)$$

where  $\epsilon$  is dielectric constant,  $c$  is capacitance,  $\epsilon_0$  dielectric permittivity of space and  $d$  is diameter of sample disk.

\* Corresponding author: mohkhairy@fsc.bu.edu.eg  
<https://doi.org/10.15251/DJNB.2022.174.1111>

Nanomaterials have been actively explored in recent years due to their intriguing physical and chemical features when compared to their bulk counterparts [5]. Several researchers have used solvothermal, hydrothermal, self-assembly, and sol-gel techniques to produce ZnO nano/microcrystals [6-10].

The defect crystal structure of ZnO, often known as n-type semiconductor, includes excess  $Zn^{2+}$  ( $Zn_{1+}$  O) that occupies interstitial spaces [11]. While NiO is a p-type semiconductor with vacancies at Ni sites ( $Ni_{1-}$ O), it has a defect structure with vacancies at Ni sites [12]. A series of solid solutions is formed by ZnO and NiO. With increasing temperature, NiO solubility in ZnO rises [13].

Nickel oxide has a rock salt structure and antiferromagnetic characteristics below 523K, making it a typical binary transition metal oxide. Numerous theoretical and practical research on NiO band structure and electronic characteristics have been conducted [14–19]. The band gap for bulk NiO was discovered to be around 4 eV, which is significantly less than the Mott-Hubbard correlation energy,  $u$  ( $u$  7–10 eV) [21, 20].

Nano-pigments are organic or inorganic compounds that are insoluble in the substrate or binders, chemically and physically inert, and have a particle size smaller than 100 nm [22]. Nano-pigments have lately obtained a wide range of industrial uses [23], despite the fact that particle sizes in the 100-200 nm range are necessary in current production practice.

The strong blue color of ZnO doped with nickel has piqued interest in a variety of applications. Despite the fact that some inorganic pigments are hazardous, they are frequently used in paints, ceramics, plastics, glazes, and glasses. ZnO-NiO compounds have hues that are acceptable for use in paints. ZnO might theoretically be rendered ferromagnetic at Curie temperature by doping it with transition metal ions (Ni, Mn, Co, V, or Fe) [24, 25]. Metal oxides' photocatalytic activity are influenced by their surface area and surface imperfections. Surface flaws are increased when a transition metal ion is doped [26, 27]. This may cause the absorption to shift towards the visible zone.

In the present study, Ni doped ZnO ( $Ni_xZn_{(1-x)}O$ , with  $20 \leq x \leq 70$ ) were fabricated by the co-precipitation method. XRD and FTIR measurements validated the structural and phase formation. Scanning electron microscopy (SEM) was used to photograph the surface morphology and particle size of the samples, as well as the variation of crystallite size with calcined temperature. At different frequencies in the range of 100 Hz - 1 MHz, the temperature dependency of dielectric constant, loss, and AC conductivity (ranged from 298 to 623 K) was investigated. The color of ZnO as a pigment was examined in relation to Ni concentration and temperature.

## 2. Experimental

### 2.1. Materials

The materials which used in our preparations are; zinc acetate [ $Zn(CH_3COO)_2 \cdot 2H_2O$ ] (98.5%) provided from Adwic, nickel nitrate [ $Ni(NO_3)_2 \cdot 6H_2O$ ] (98%) provided from BDH, oxalic acid [ $H_2C_2O_4 \cdot 2H_2O$ ] (100%) provided from BDH, Glaze. Double distilled water was used throughout all the experiments.

### 2.2. Materials Preparations

#### 2.2.1. Preparation of pure ZnO

ZnO was synthesized by slowly adding 250 ml of 0.15M of Oxalic acid [ $H_2C_2O_4 \cdot 2H_2O$ ] to 100 ml of 0.1 M zinc acetate [ $Zn(CH_3COO)_2 \cdot 2H_2O$ ] and stirring at 150 rpm for 12 hours at room temperature. To remove contaminants, the zinc oxalate precipitate was filtered and rinsed with distilled water at least three times before being dried at 120 °C for 1 hour, and then calcined at 400 °C, 600 °C, 800 °C and 1000 °C for each temperature respectively, for 2h. The samples were denoted as  $Zn_{400}$ ,  $Zn_{600}$ ,  $Zn_{800}$ ,  $Zn_{1000}$ .

#### 2.2.2. Preparation of ZnO-NiO pigment

This pigment was prepared with different concentration of nickel nitrate (20%, 40%, 70%) by taking 100 ml of 0.1M of zinc acetate [ $Zn(CH_3COO)_2 \cdot 2H_2O$ ] and 0.1M of nickel nitrate

[Ni(NO<sub>3</sub>)<sub>2</sub>·6H<sub>2</sub>O] with (20%) concentration and at room temperature, slowly add 250 ml of 0.15M oxalic acid [H<sub>2</sub>C<sub>2</sub>O<sub>4</sub>·2H<sub>2</sub>O] with a steady stirring rate of 150 rpm for 12 hours. To remove contaminants, the precipitate was filtered and rinsed with distilled water at least three times before being dried at 120 °C for one hour. And then it was calcined at 400, 600, 800 and 1000 °C for each temperature respective, for 2h. All other concentrations were prepared by the same procedure. The samples were denoted as Z2N<sub>400</sub>, Z2N<sub>600</sub>, Z2N<sub>800</sub>, Z2N<sub>1000</sub>, Z4N<sub>400</sub>, Z4N<sub>600</sub>, Z4N<sub>800</sub>, Z4N<sub>1000</sub>, Z7N<sub>400</sub>, Z7N<sub>600</sub>, Z7N<sub>800</sub> and Z7N<sub>1000</sub> for samples with 20, 40 and 70 % of Ni at 400, 600, 800 and 1000 °C, respectively.

The color of the obtained pigments were photographed after the following procedures; definite weight of the prepared samples mixed with past of glaze and pasted on the ceramic and then calcined 900 °C for 1h.

### 2.3. Characterization Techniques

Philips PW-3710 diffractometer with monochromated Cu K radiation wave-length ( $\lambda = 1.5406 \text{ \AA}$ ) was used to perform X-ray powder diffraction (XRD) at room temperature. A scanning electron microscope was used to conduct morphological research (SEM, JEOL-JSM 6360 unit).

The electrical properties (The electrical conductivity, dielectric constant and dielectric loss) were measured for metal oxide samples. The electrical measurements were evaluated a in frequency range from 300 Hz to 1 MHz t a constant voltage (1 volt) in temperature range from 298 to 623 K, by means of programmable automatic LCR bridge (model RM6306 Philips Bridge).

Ultra Scan Pro, Hunter lab Spectrophotometer were used to measurement L\*, a\*, b\*, c\*, h, for prepared samples. The L\* (lightness) axis is 0 for black and 100 for white. Positive values are red, negative values are green, and 0 is neutral on the -a\* (red-green) axis. Positive values are yellow, negative values are blue, zero is neutral on the -b\* (blue-yellow), and h represents the hue.

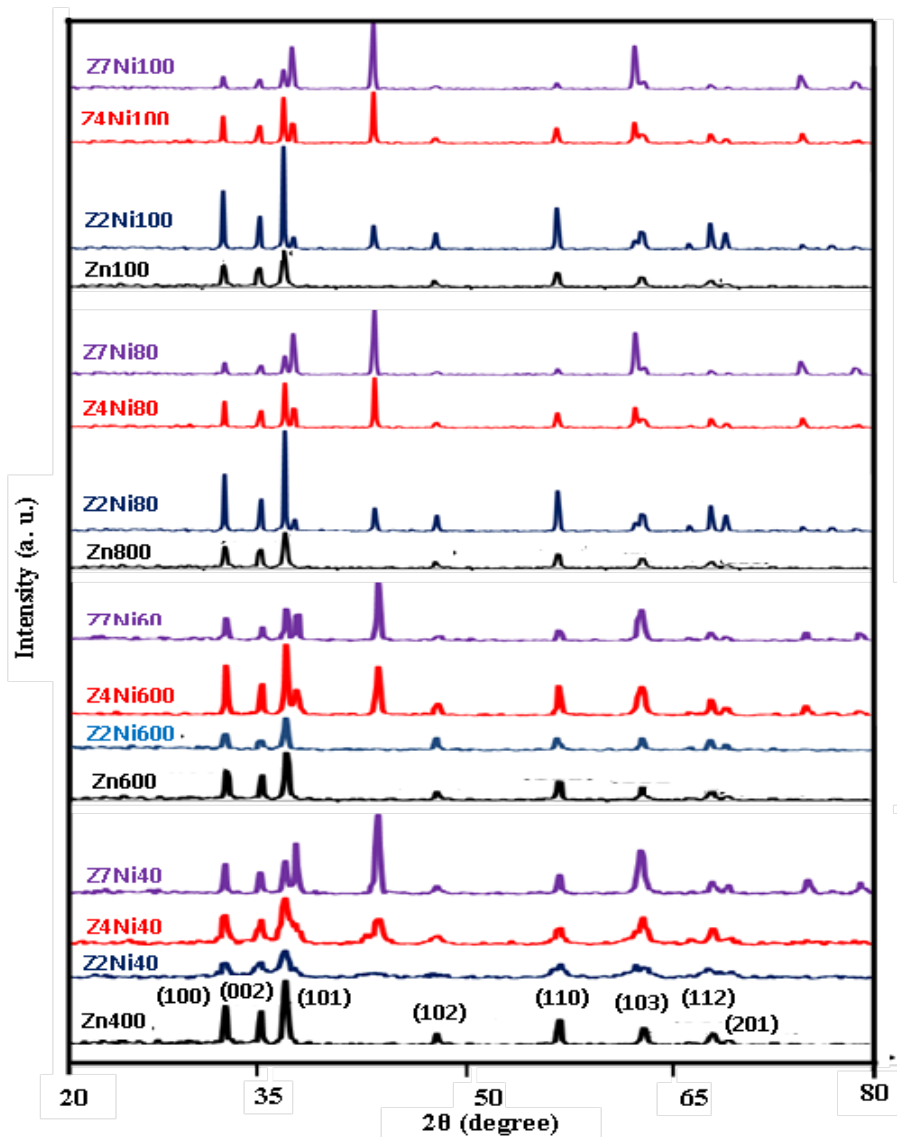
## 3. Results and Discussion

### 3.1. X – ray diffraction

XRD patterns of Ni<sup>+2</sup> doped ZnO oxide with Ni content (x= 0.2, 0.4, and 0.7) calcined at 400, 600, 800, and 1000 °C are shown in Fig.1. The intense diffraction peaks of ZnO are found at 31.77, 34.43, 36.27, 47.35, 56.61, and 62.83, respectively, related to the (100), (002), (101), (102), (110), and (103) planes. The formation of the hexagonal Wurtzite structure ZnO (space group: P6<sub>3</sub>mC (186) as indexed in the standard data (JCPDS card No. 36-1451, a = 3.249 Å and c = 5.206 Å) is clearly seen in the XRD pattern of these samples. This indicates that the crystal structure of ZnO is not modified due to the presence of NiO. The prominent (002) plane is observed in all samples, which is less or more dense plane. Such changes are to be expected that Zn<sub>60</sub>Ni<sub>40</sub> (Z4N) is preferentially oriented along (002) plane. The peak orientation is shifted from (002) plane to (100) with 40 and 70 mole% which calcined at 800 and 1000 °C as shown in Table 1. It was revealed that (from 20 and 70% mole) the ZnO peaks intensity were decreased which was attributed to the decreasing in the crystallinity of ZnO causing increases of the electrical conductivity (high defects). The shift in the (002) peak for Ni doped ZnO might be due to the substitution of Zn by NiO in hexagonal lattice [28]. These shifts are consistent with the findings of the earlier study [29, 30]. Variations in the atomic environment caused by extrinsic doping of ZnO samples could explain the shift in crystallinity [29, 30].

Table 1. Peak orientation data for  $Ni_xZn_{(1-x)}O$  samples.

| Samples | Peak orientation% |       |       |        |
|---------|-------------------|-------|-------|--------|
|         | plane             | 600°C | 800°C | 1000°C |
| Z2Ni    | (100)             | 63.7  | 56.9  | 65.2   |
|         | (002)             | 45.0  | 47.9  | 48.4   |
| Z4Ni    | (100)             | 65.4  | 50.0  | 55.9   |
|         | (002)             | 52.0  | 47.2  | 44.1   |
| Z7Ni    | (100)             | 64.1  | 55.0  | 60.0   |
|         | (002)             | 47.1  | 40.0  | 40.0   |

Fig. 1. XRD patterns of  $Ni_xZn_{(1-x)}O$  samples at different Ni content.

It was also observed that, an additional diffraction peak correspond to NiO comes into existence at an angle  $2\theta \approx 43.2$  are slightly shifted to  $\theta \approx 42.9$  which clearly indicate that a modified phase cubic solid solution (Zn-Ni)O [31, 32]. Additional when  $x$  was increased from 40 to 70 mole% the NiO (111) peak could be more intense in the XRD pattern of samples. This intense peak in the XRD spectra is corresponding to the remaining un-reacted NiO. That is to say that,

phase segregation has started in the system calcined 800°C and the solubility of Ni<sup>2+</sup> ion in Zn<sub>1-x</sub>Ni<sub>x</sub>O has decreased. Figure 2 depicts the influence of annealing temperature on the crystallinity of the samples. The X-ray diffraction patterns of Ni doped ZnO samples at varied annealing temperatures of 400, 600, 800, and 1000 degrees Celsius are shown in this figure. Annealing improves crystallinity significantly, resulting in more intense and sharper XRD peaks. The ZnO (002) peak shift exists after annealing at 600°C, however it is shifting to the right. Furthermore, the standard peak position of ZnO powders (34.43°) found between those of the peak position (34.2°) and (34.59°) implying that the lattice constant *c* is shortened in the annealed samples [33]. Furthermore, due of the favored orientation during annealing at 600°C, grain growth can alter in the peak intensity of (002). The crystallite size  $D_{\text{XRD}}$  of ZnO and Ni<sub>x</sub>Zn<sub>(1-x)</sub>O at different calcination temperatures was calculated based on main diffraction peak ( $\theta=34.43^\circ$ ) by using Scherer's equation [34]:

$$D_{\text{XRD}} = k\lambda/\beta\cos\theta \quad (2)$$

where *k* is a constant (having the value of 0.9 in our case),  $\lambda$  is the X-ray wavelength,  $\theta$  is the angle of the diffraction and  $\beta$  is the full width at half maximum of the diffraction peak. The growth in crystalline size due to thermal treatment temperature is shown in Table 2. The average Zn<sub>1-x</sub>Ni<sub>x</sub>O nano phase crystallite size varied from 40 to 125 nm.

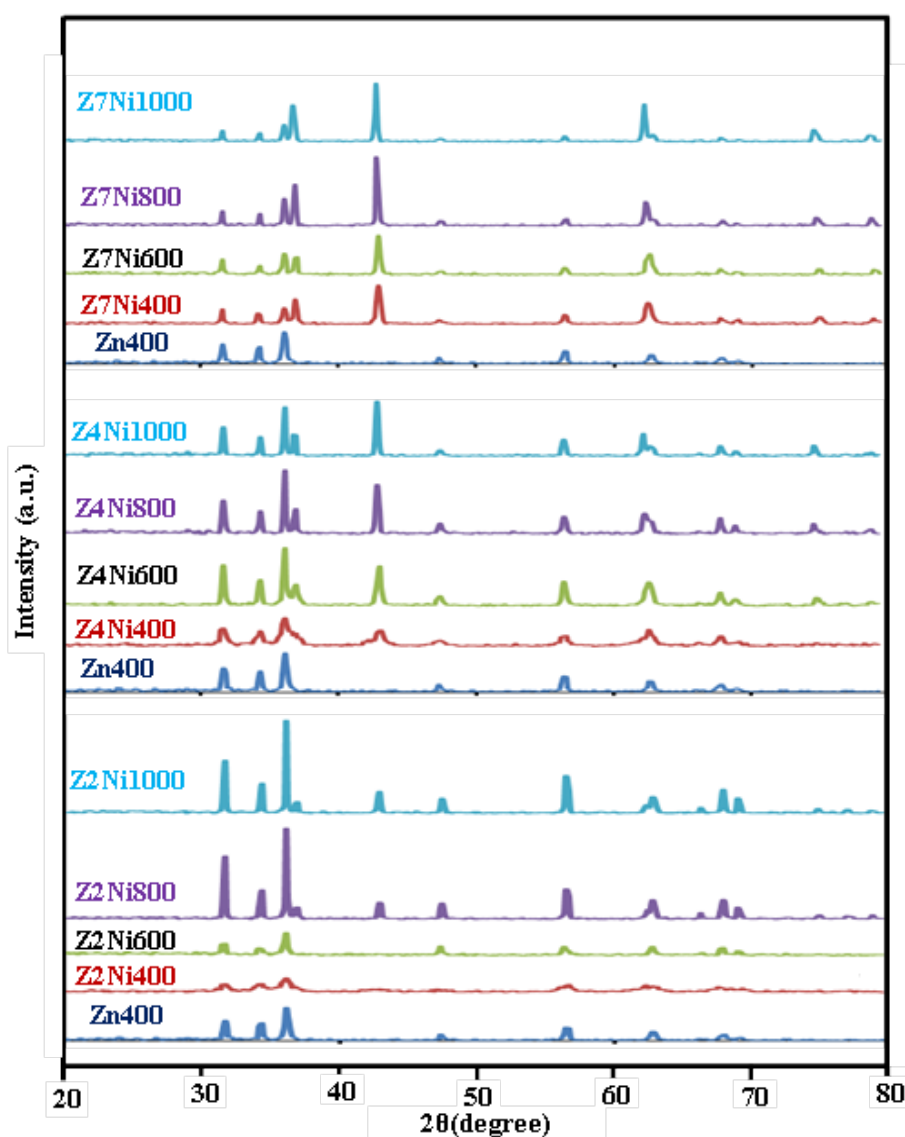


Fig. 2. XRD patterns of Ni<sub>x</sub>Zn<sub>(1-x)</sub>O samples at different calcinations temperature.

Table 2. XRD data for  $Ni_xZn_{(1-x)}O$  samples.

| Sample              | Crystallites Size $D_{XRD}$ (nm) | Lattice Constant ( $\text{\AA}$ ) |      | a/c  |
|---------------------|----------------------------------|-----------------------------------|------|------|
|                     |                                  | a                                 | c    |      |
| Z400                | 38                               | 3.24                              | 4.86 | 0.67 |
| Z600                | 49                               | 3.26                              | 5.21 | 0.63 |
| Z1000               | 88                               | 3.26                              | 5.21 | 0.63 |
| Z2N <sub>400</sub>  | 13                               | 3.25                              | 5.22 | 0.62 |
| Z2N <sub>600</sub>  | 47                               | 3.25                              | 5.22 | 0.62 |
| Z2N <sub>800</sub>  | 90                               | 3.25                              | 5.22 | 0.62 |
| Z2N <sub>1000</sub> | 109                              | 3.25                              | 5.20 | 0.63 |
| Z4N <sub>400</sub>  | 21                               | 3.25                              | 5.21 | 0.62 |
| Z4N <sub>600</sub>  | 47                               | 3.25                              | 5.21 | 0.62 |
| Z4N <sub>800</sub>  | 78                               | 3.25                              | 5.21 | 0.62 |
| Z4N <sub>1000</sub> | 93                               | 3.25                              | 5.21 | 0.62 |
| Z7N <sub>400</sub>  | 85                               | 3.25                              | 5.21 | 0.62 |
| Z7N <sub>600</sub>  | 50                               | 3.25                              | 5.27 | 0.62 |
| Z7N <sub>800</sub>  | 80                               | 3.2                               | 4.77 | 0.67 |
| Z7N <sub>1000</sub> | 80                               | 3.25                              | 5.2  | 0.63 |

### 3.2. SEM

SEM was utilized to look the detailed morphology of Ni doped ZnO sample. Fig 3 show SEM images of  $Zn_{1000}$ ,  $Zn_2Ni_{400}$ ,  $Zn_2Ni_{600}$ ,  $Zn_2Ni_{1000}$ ,  $Zn_7Ni_{400}$ ,  $Zn_7Ni_{600}$  and  $Zn_7Ni_{1000}$  samples.

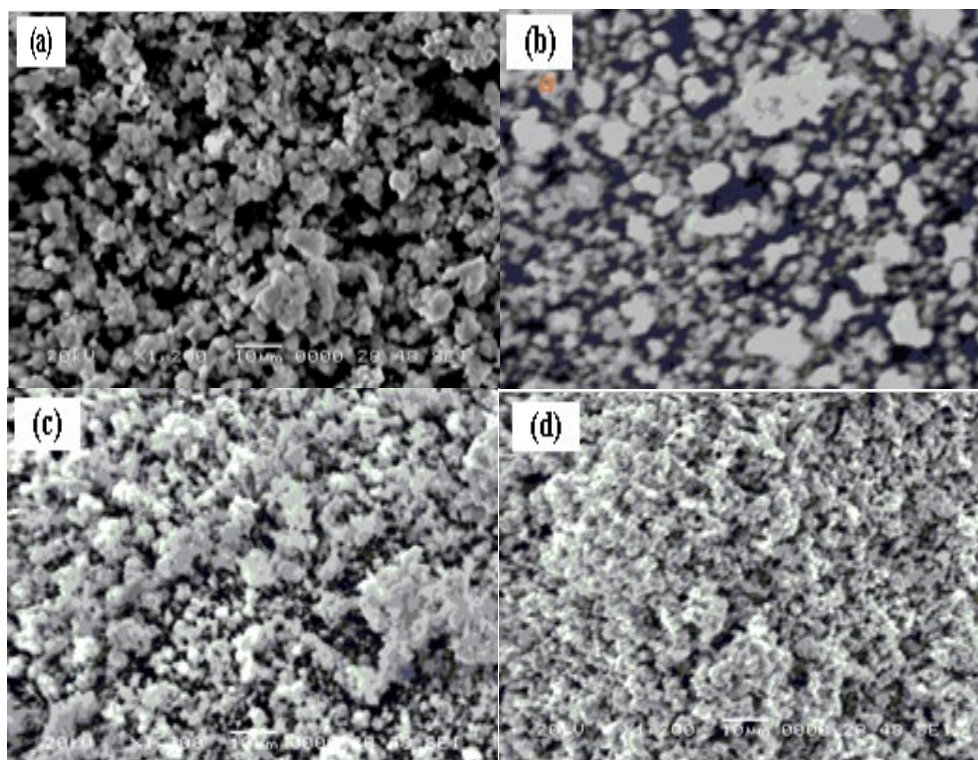


Fig. 3.1 SEM images of NiO-ZnO samples: a)  $Zn_{1000}$ , b)  $Zn_2Ni_{400}$ , c)  $Zn_2Ni_{600}$ , d)  $Zn_2Ni_{1000}$ .

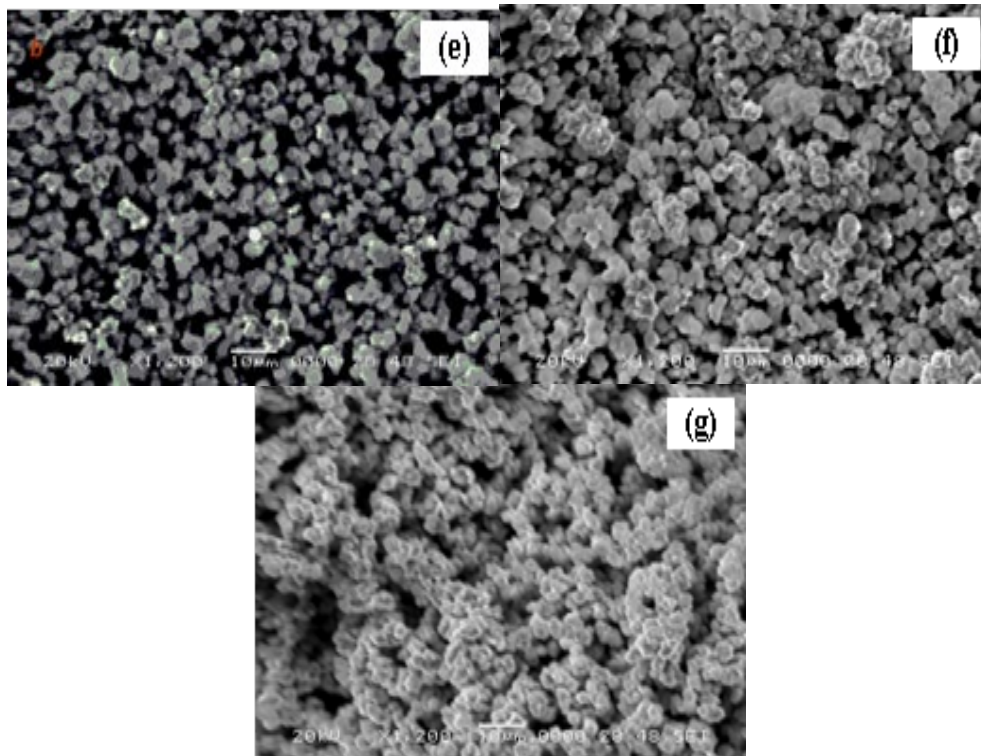


Fig. 3.2. SEM images of NiO-ZnO samples: e)  $Zn_7Ni_{400}$ , f)  $Zn_7Ni_{600}$ , g)  $Zn_7Ni_{1000}$ .

The images reveal high homogeneity at the surface with a lot of particle agglomeration. The particles are nearly spherical shape and uniform in size. The increasing of calcination temperature as well as increasing the Ni content from 20% to 70% show increasing of particle size and enhance the aggregation of particles. Microstructure evolution in the sample is relative of strong change in the composition and crystallizes during annealing process.

### 3.3. Electrical Properties

#### 3.3.1. AC conductivity

The effect of temperature on the AC conductivity for Zn600, Z4N600, and Z7N600 samples in the temperature range of 298 K to 623 K in the frequency range of  $10^2$ - $10^6$  Hz is shown in Fig. 4. Plotting the logarithm of AC conductivity vs the inverse temperature  $1000/T$  yielded the Arrhenius plot. Using the relationship, the activation energy of the samples was determined.

$$\sigma = \sigma_0 \exp(-E_a/K_B T) \quad (3)$$

In which  $K_B$  is the Boltzmann const and  $\sigma_0$  is the pre exponential factor. The activation energy of the samples was determined to be between 0.22 and 0.49 eV. The fact that AC conductivity is temperature dependent shows that electrical conduction in the material is a thermally stimulated process.

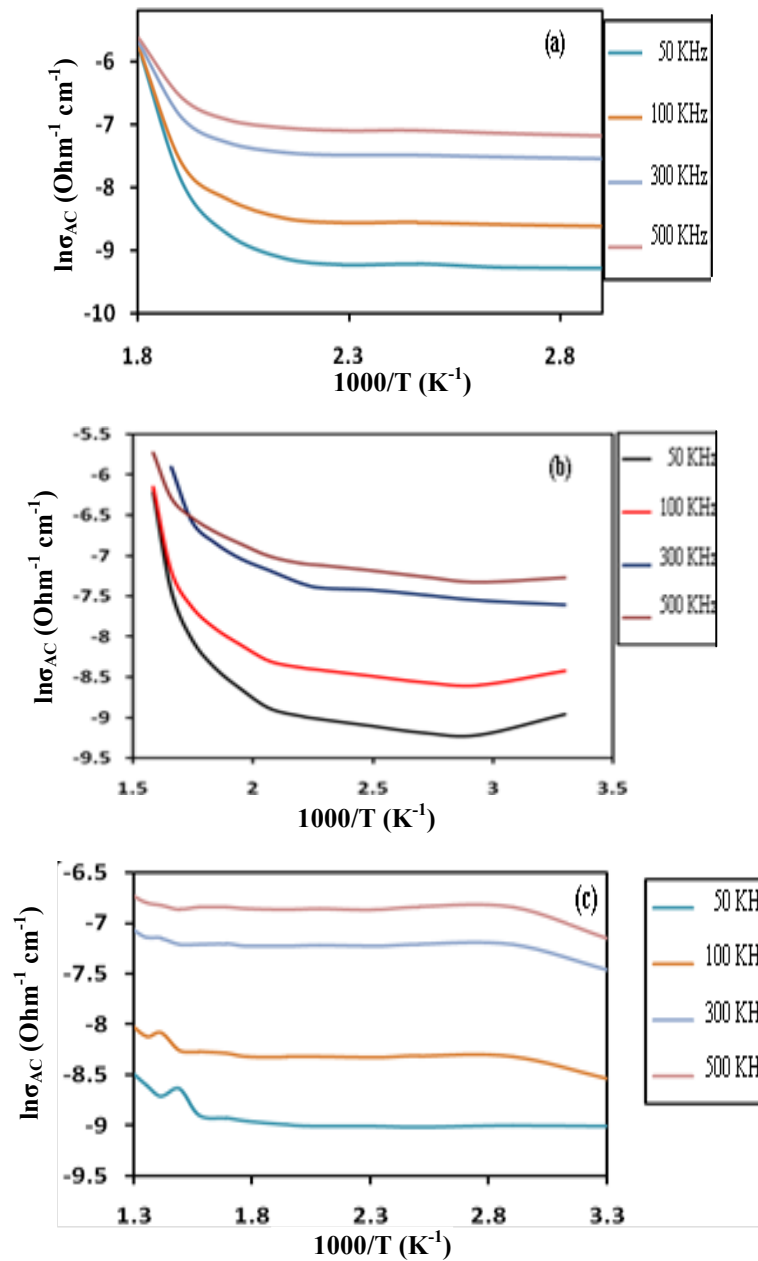


Fig. 4. Temperature dependence of AC conductivity of: a) Zn<sub>600</sub>, b) Z4N<sub>600</sub> and c) Z70N<sub>600</sub>.

It can be seen that the  $\sigma_{AC}$  of ZnO samples increases as the temperature increases. The natural features of ZnO (oxygen vacancies and interstitial Zn atoms) are well known to be created at high temperatures using the following equations:



Two additional electrons are added to the carrier concentration after ionization [38]. The electrical conductivity of ZnO increases as the temperature rises. This occurs when the electron or hole moves from one localized site to the next during the electrical conduction of doped ZnO [39]. The conductivity of the ZnO increases somewhat as the Ni concentration rises (Table 3). Under the



effect of the tetrahedral crystal field of ZnO [40], the Ni-d-states emerging near the EF can be divided into  $e_g$  and  $t_{2g}$  states. The  $t_{2g}$  state after hybridization with the valence band's p orbital [41].

The activation energy  $E_a$  was calculated from the relation (3). The value of  $E_a$  were calculated at different frequency and given in Table 3. It was discovered that the electronic contribution dominates weak activation energies (hopping over barriers between neighboring localized state). Similar conductivity fluctuations have been documented [42]. The activation energy of NiO – ZnO samples was found to be lower than that of ZnO. Because of the donor concentration and impurity levels, the activation energy falls with NiO doping concentration. The Fermi level rises in the energy gap as donor carrier concentration rises, resulting in a drop in activation energy. The rise in conductivity with frequency may be an indication of trapped charges being released in the disorder system. The nano crystallite nature of the samples contributes to this.

Table 3. The effect of Ni content on the conductivity and the dielectric constant of  $Ni_xZn_{(1-x)}O$ .

| Sample            | $\sigma$<br>at 25°C   | $\epsilon'$ |        |       | Ea (ev) |        |       |
|-------------------|-----------------------|-------------|--------|-------|---------|--------|-------|
|                   |                       | 600Hz       | 100KHz | 1 MHz | 600Hz   | 100KHz | 1 MHz |
| Zn <sub>600</sub> | $3.04 \times 10^{-6}$ | 21          | 35.1   | 28.7  | 0.49    | 0.34   | 0.25  |
| Z4Ni              | $1.29 \times 10^{-4}$ | 42          | 23.5   | 22.7  | 0.40    | 0.32   | 0.24  |
| Z7Ni              | $7.14 \times 10^{-4}$ | 37.7        | 32.5   | 26.7  | 0.34    | 0.25   | 0.22  |

### 3.3.2. Dielectric properties

Figure 5 shows the effect of temperature on the dielectric constant ( $\epsilon'$ ) of Zn600, Z4N600, and Z7N600 samples. At lower frequencies, the increase in the dielectric constant with temperature is more visible. It was discovered that as the temperature of the samples rises, the dielectric constant of the samples rises as well. At low temperatures, molecular dipoles in polar materials cannot orient themselves (dipole freezes). The dipoles' orientation is assisted as the temperature rises, increasing the dielectric constant'. It's also worth noting that the number of space charge carriers influences the polarization of space charge carriers. The number of carriers increases as the temperature rises, resulting in a greater build-up of space charge polarization and thus improved dielectric characteristics.

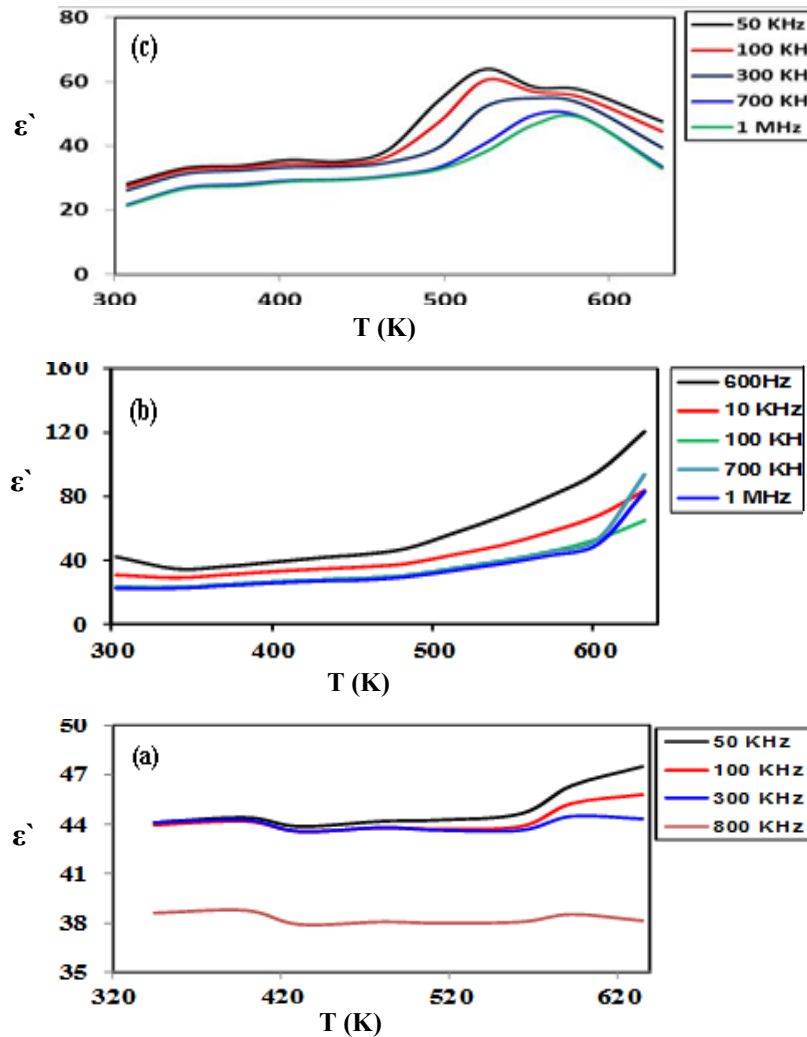


Fig. 5. Temperature dependence of dielectric constant of: a)  $Zn_{600}$ , b)  $Z4N_{600}$  and c)  $Z70N_{600}$ .

The contribution of the multicomponent polarizability (ZnO, NiO, and (Zn – Ni)O solid solution), which is deformational and relaxation, can be attributed to the decrease in dielectric permittivity with frequency. Under the applied field, deformational polarizability is defined as the mutual displacement of oppositely charged particles.

Figure 6 depicts the fluctuation in dielectric loss ( $\epsilon''$ ) as a function of temperature for the investigated materials. At higher temperatures and lower frequencies,  $\epsilon''$  exhibit substantial temperature dependency, as shown in this diagram.

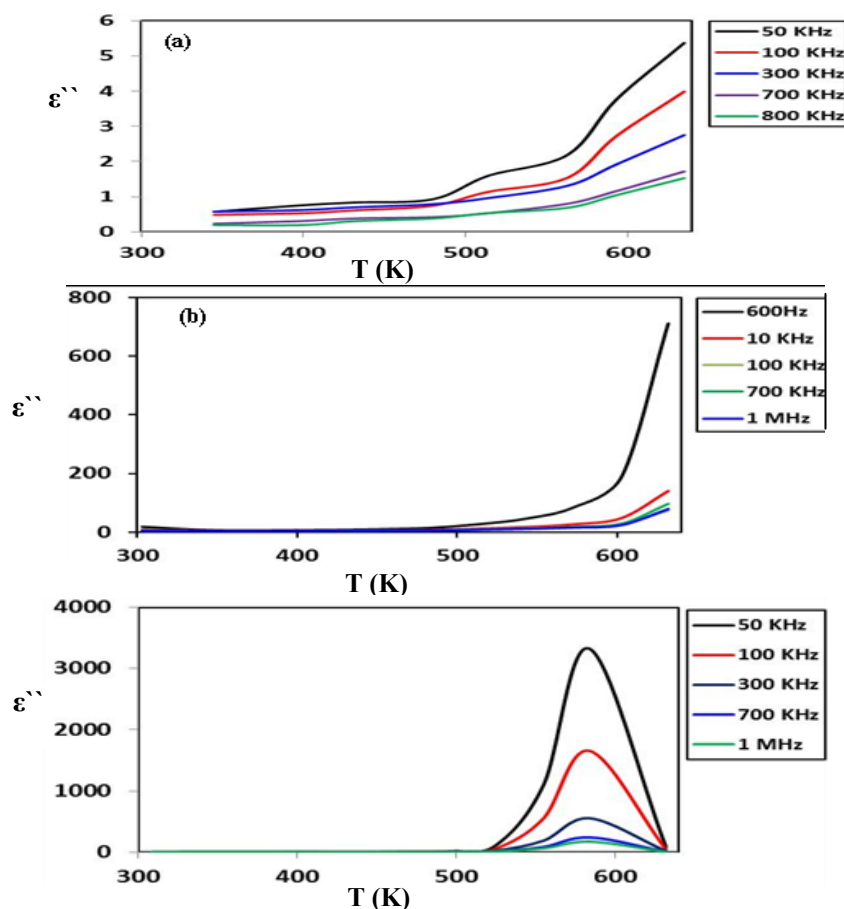


Fig. 6. Temperature dependence of dielectric loss of: a)  $Zn_{600}$ , b)  $Z4N_{600}$  and c)  $Z70N_{600}$ .

It was discovered that when the frequency increases, the  $\epsilon''$  drops. The fact that the dielectric constant and dielectric loss decrease with frequency suggests that ZnO crystals have varied widths of domains and thus variable relaxation times [43].

It's worth noting that the extremely high values of  $\epsilon'$  and  $\epsilon''$  at low frequencies could be owing to probable dielectric amplification caused by conducting grain boundaries covering insulating grains. It should be mentioned here that the values of  $\epsilon'$  and  $\epsilon''$  increases with increasing the Ni content indicating the contribution of NiO in the increasing the polarization in ZnO crystals.

### 3.4. Color properties









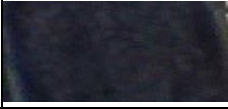

The color properties of  $Ni_xZn_{(1-x)}O$  ( $x = 0.2, 0.4$  and  $0.7$ ) calcined at 600 and 1000 °C have been investigated by using the CIELAB and coordinates. Table 4 shows the result of the colorimetric coordinates  $L^*$ ,  $a^*$ ,  $b^*$ . The results show that the calcinations of samples at temperatures 600 and 1000 °C (Table 4) had caused the formation of dark blue pigment which is due to the inclusion of Ni in ZnO structure from this table shown that  $Zn_{0.8}Ni_{0.2}$  have very good blue hue ( $L^*=45.18$ ,  $a^*=13.26$ ,  $b^*=-38.74$ ).

Table 4 shows however the important comparison of different pigment is the evolution of pigment chroma  $C^*$  and hue ( $h^*$ ). The results indicate that  $C^*=41.14$ ,  $h^*=288.8$  have larger value of  $h^*$  than that of the all before references samples which could be the consequence of a better solid solution between ZnO and NiO [44]. Table 5 shows the color of this samples calcined at 600 °C at all different  $Ni^{+2}$  ratios (from 20 to 70 mole %) have more intense color than the samples which are calcined at 1000 °C this is due to the sintering process. Furthermore by increasing the concentration of  $Ni^{+2}$  ions the dark blue color of the samples were decreases from (20 to 70 mole %). This is due to the remaining un-reacted NiO.

Table 4. Colorimetric data for  $Ni_xZn_{(1-x)}O$  samples.

| Sample              | CIE Lab/Colorimetric data |       |       |
|---------------------|---------------------------|-------|-------|
|                     | L*                        | a*    | b*    |
| Z2N <sub>400</sub>  | 33.57                     | 18.06 | -37.7 |
| Z2N <sub>600</sub>  | 45.18                     | 13.26 | -38.7 |
| Z2N <sub>1000</sub> | 27.15                     | 8.56  | -17.6 |
| Z2N <sub>400</sub>  | 28.96                     | 12.16 | -24.7 |
| Z4N <sub>600</sub>  | 30.21                     | 10.88 | -24.2 |
| Z4N <sub>1000</sub> | 27.9                      | 9.51  | -20.4 |
| Z7N <sub>400</sub>  | 28.08                     | 9.02  | -11.2 |
| Z7N <sub>600</sub>  | 30.92                     | 7.21  | -17   |
| Z7N <sub>1000</sub> | 28.22                     | 6.05  | -14.4 |
| Ni <sub>1000</sub>  | 29.14                     | 6.36  | -15   |

Table 5. Colorimetric data for  $Ni_xZn_{(1-x)}O$  samples.

| Sample              | L*    | C*    | h     | Photo  |
|---------------------|-------|-------|-------|--|
| Z2N <sub>400</sub>  | 33.57 | 41.8  | 295.6 |   |
| Z2N <sub>600</sub>  | 45.18 | 41.14 | 288.8 |  |
| Z2N <sub>1000</sub> | 27.15 | 19.54 | 296   |  |
| Z4N <sub>400</sub>  | 28.96 | 27.55 | 296.2 |  |
| Z4N <sub>600</sub>  | 30.21 | 26.56 | 294.2 |  |
| Z4N <sub>1000</sub> | 27.9  | 22.54 | 295   |  |
| Z7N <sub>400</sub>  | 28.08 | 19.42 | 297.7 |  |
| Z7N <sub>600</sub>  | 30.92 | 18.45 | 293   |  |
| Z7N <sub>1000</sub> | 28.22 | 15.63 | 292.8 |  |
| Ni <sub>1000</sub>  | 29.14 | 16.26 | 293   |  |

#### 4. Conclusion

Nanosized Ni doped ZnO ( $\text{Ni}_x\text{Zn}_{1-x}\text{O}$ , with  $(20 \leq x \leq 70)$  were prepared by co-precipitation method. The results of the XRD and SEM obviously show that  $\text{Ni}^{2+}$  ions easily integrate into the ZnO structure. For the highest concentration of  $\text{Ni}^{2+}$  for  $x = 0.40$  and  $0.70$  of  $\text{Ni}^{2+}$  doping, the XRD revealed an additional NiO – associated diffraction peak, indicating an upper limit of Ni concentration. The crystallite size was discovered to be between 13 and 109 nm. With the addition of Ni to the solution, the temperature dependency of electrical conductivity of samples increases. The temperature dependence of dielectric consist of samples is found to decrease with incorporation of Ni in the ZnO. The samples show very good blue color with load 20% of Ni.

#### References

- [1] H. Chen, P. Li, H. Zhou, W. Zhang, L. Cong, J. Ma, Mater. Res. Bull.146, 111572 (2022); <https://doi.org/10.1016/j.materresbull.2021.111572>
- [2] E. Peksu, H. Karaagac, J. Alloys Compds. 884, 61124 (2021); <https://doi.org/10.1016/j.jallcom.2021.161124>
- [3] L. H. Cheng, L.Y. Zheng, L. Meng, G.R. Li, Y. Gu, F. P. Zhang, R. Q. Chu, Z. J. Xu, Ceram. Intern. 38 (1), S457-S461 (2012); <https://doi.org/10.1016/j.ceramint.2011.05.039>
- [4] H. Jiang, X. Ren, X. Lao, A. Kong, M. Zhong, Y. Sun, Y. Wu, Z. Yao, L. Shi, J. Europ. Ceram. Soc. 42 (9), 3898-3904 (2022); <https://doi.org/10.1016/j.jeurceramsoc.2022.03.033>
- [5] C. Liewhiran, S. Seraphin, S. Phanichphant, Appl. Phys. 6 (3), 499-502 (2006); <https://doi.org/10.1016/j.cap.2005.11.047>
- [6] G. Li, B. Wang, Y. Liu, T. Tan, X. Song, H. Yan, Appl. Surf. Sci.255 (5), 3112-3116 (2008); <https://doi.org/10.1016/j.apsusc.2008.08.107>
- [7] M. A. Mousa, W. A. A. Bayoumy, M. Khairy, Mater. Res. Bull. 48, 4576-4582 (2013); <https://doi.org/10.1016/j.materresbull.2013.07.050>
- [8] M. S. Kim, D. Y. Kim, M. Y. Cho, G. Nam, S. Kim, D. Lee, S. Kim, J. Y. Leem, Vacuum 86 (9) 1373-1379 (2012); <https://doi.org/10.1016/j.vacuum.2012.01.006>
- [9] A. Marcu, L. Trupina, R. Zamani, J. Arbiol, C. Grigoriu, J.R. Morante, Thin Solid Films 20 (14), 4626-4631 (2012); <https://doi.org/10.1016/j.tsf.2011.10.126>
- [10] G. Zhu, T. Lv, L. Pan, Z. Sun, Ch. Sun, J. Alloys Compd. 509 (2), 362-365 (2011); <https://doi.org/10.1016/j.jallcom.2010.09.026>
- [11] J. Jokela, Stability And Structure Of Hydrogen defects In Zinc Oxide, Ph.D) 2005).
- [12] M. D. Irwin, D. B. Buchholz, A. W. Hains, R. P. H. Chang, T. J. Marks, PANS, 105 (8), (2008) 2783-2787; <https://doi.org/10.1073/pnas.0711990105>
- [13] A.N. Baranov, P.S. Sokolov, O.O. Kurakevich, V.A. Tafeenk D. Trots, V.L. Solozhenko, High Press. Res. 28, 515-519 (2008); <https://doi.org/10.1080/08957950802379307>
- [14] X. Wen, Z. Ran, R. Zheng, D. Du, C. Zhao, R. Li, H. Xu, T. Zeng, C. Shu, J. Alloys Compds. 901, 163703 (2022); <https://doi.org/10.1016/j.jallcom.2022.163703>
- [15] F. Yang, X. Zhang, L. Zhou, S. Lin, X. Cao, J. Jiang, X. Lu, Chem. Engin. J. 432(15), 134255 (2022); <https://doi.org/10.1016/j.cej.2021.134255>
- [16] K. O. Egbo, S. K. Shil, C. G. Kwok, Y. Wang, C. P. Liu, K. M. Yu, J. Alloys Compds. 876, 160136 (2021); <https://doi.org/10.1016/j.jallcom.2021.160136>
- [17] F. Chen, Y. Chi, H. Zhang, F. Ma, F. Qin, J. Alloys Compds. 888, 161463 (2021); <https://doi.org/10.1016/j.jallcom.2021.161463>
- [18] L. Ru-song, X. Du-qiang, H. Shi-qi, W. Zhi-jian, H. Ling, Z. Xiao-hua, Chin. J. Phys. 56(6), 2829-2836 (2018).
- [19] Y. H. Elbashar, S. S. Moslem, H. H. Hassan, D. A. Rayan, Phosphorus Sulfur Silicon Relat. Elem. 196(1), 61-70 (2021); <https://doi.org/10.1080/10426507.2020.1800703>
- [20] N. M. Hosny, Polyhedron 30, 470-476 (2011); <https://doi.org/10.1016/j.poly.2010.11.020>

- [21] S. Hufner, P. Steiner, I. Sander, M. Neumann, and S. Witzel, *Z. Phys. B: Condens. Matter*. B 83, 185-192(1991); <https://doi.org/10.1007/BF01309416>
- [22] F. M. Nejad, S. Baghshahi, S. Baghshahi, L. Bakhtiari, *Trans. Indian Ceram. Soc.* 70(2), 93-99 (2013); <https://doi.org/10.1080/0371750X.2011.10600154>
- [23] Z. Hu, M. Xue, Q. Zhang, Q. Sheng, Y. Liu, *Dyes Pig.* 76, 173-178 (2008); <https://doi.org/10.1016/j.dyepig.2006.08.026>
- [24] T. Diell, H. Ohno, F. Matsukura, J. Cibert, D. Ferrand, *Science* 287, 1019-1022 (2000); <https://doi.org/10.1126/science.287.5455.1019>
- [25] K. Sato, H. Katayama-yoshida, *Jpn. J. Appl. Phys., Part 2*, 39, (2000) L555-L558; <https://doi.org/10.1143/JJAP.39.L555>
- [26] Li, Y. Zij, Xi, Hu, XL, *Langmuir*, 26, 591-597 (2010); <https://doi.org/10.1021/la902117c>
- [27] R. X. Wang, J. H. Yang, Y. Liu, H. Xu, L. Hu, *Appl. Surface. Sci.*, 227, 312-317 (2004); <https://doi.org/10.1016/j.apsusc.2003.12.012>
- [28] B. Zhang, X. Zhang, H. Gong, Z. Wu, S. Zhou, Z. Du, *Phys. Lett. A* 372, 2300-2303 (2008); <https://doi.org/10.1016/j.physleta.2007.11.046>
- [29] S. P. Lau, S. F. Yu, H. Y. Yang, L. Wang, M. Tanemura, J. S. Chen, *Appl. Phys. Lett.* 90, 032509-0325012 (2007); <https://doi.org/10.1063/1.2433028>
- [30] O. Lupan, Th. Pauporté, T. Le Bahers, B. Viana, I. Ciofini, *Adv. Funct. Mater.* 21(18), 3564-3572 (2011); <https://doi.org/10.1002/adfm.201100258>
- [31] Z. Wei, H. Qiao, H. Yang, C. Zhang, X. Yan, *J. Alloys Compds.* 479, 855-858 (2009); <https://doi.org/10.1016/j.jallcom.2009.01.064>
- [32] H. Kedesdy, A. Drukalsky, *J. Am. Chem. Soc.* 76, 5941-5946 (2008); <https://doi.org/10.1021/ja01652a013>
- [33] X. J. Liu, C. Song, F. Zeng, X. B. Wang, F. Pan, *Appl. Phys.* 40, 1608-1613 (2007); <https://doi.org/10.1088/0022-3727/40/6/003>
- [34] H.P. Klug, L.E. Alexander, *X-ray diffraction procedures for polycrystalline and amorphous materials*, Wiley, New York 193-197 (1970).
- [35] E. Lavat, C. C. Wagner, J. E. Tasca, *Ceram. Inter.* 34, 2147-2153 (2008); <https://doi.org/10.1016/j.ceramint.2007.09.003>
- [36] R. A. Nyquist, R. O. Kagel, *Handbook of Infrared and Raman Spectra of Inorganic Compounds and Organic Salts*, Academic Press, San Diego, 4, 221 (1997).
- [37] V. Biju and M. Abdul khadar, *Spectroch. Acta Part A*, 59, 121-134 (2003); [https://doi.org/10.1016/S1386-1425\(02\)00120-8](https://doi.org/10.1016/S1386-1425(02)00120-8)
- [38] F. Kayaci, S. Vempati, I. Donmez, N. Biyikli, T. Uyar, *Nanoscale* 6, 10224 (2014); <https://doi.org/10.1039/C4NR01887G>
- [39] H. Colak, O. Türkoğlu, *J. Mater. Sci. Tech.* 28, 268-274 (2012); [https://doi.org/10.1016/S1005-0302\(12\)60052-8](https://doi.org/10.1016/S1005-0302(12)60052-8)
- [40] M. Girtan, G. G. Rusu, S. D. S. Seignon, M. Rusu, *Appl. Surf. Sci.* 254 (13), 4179-4185 (2008); <https://doi.org/10.1016/j.apsusc.2007.12.055>
- [41] H. Colak, O. Türkoğlu, *J. Mater. Sci. Technol.*, 27(10), 944-950 (2011); [https://doi.org/10.1016/S1005-0302\(11\)60168-0](https://doi.org/10.1016/S1005-0302(11)60168-0)
- [42] A. V. Luthra, *Ceram. Intern.* 40, 14927-14932 (2014); <https://doi.org/10.1016/j.ceramint.2014.06.089>
- [43] B. Want, F. Ahmad, P. N. Kotru, *Mater. Sci. Eng.*, 443 (1-2), 270-276 (2007); <https://doi.org/10.1016/j.msea.2006.09.017>
- [44] P. Sulcova, M. Trojan, *Dyes Pigm.* 4, 83-86 (1998); [https://doi.org/10.1016/S0143-7208\(98\)00036-9](https://doi.org/10.1016/S0143-7208(98)00036-9)